

2 **Determination of muon momentum in the**
3 **MicroBooNE LArTPC using an improved model of**
4 **multiple Coulomb scattering**

5 **The MicroBooNE Collaboration**

6 ABSTRACT: We discuss a technique for measuring a charged particle's momentum by means of
7 multiple Coulomb scattering (MCS) in the MicroBooNE liquid argon time projection chamber
8 (LArTPC). This method does not require the full particle ionization track to be contained inside of
9 the detector volume as other track momentum reconstruction methods do (range-based momentum
10 reconstruction and calorimetric momentum reconstruction). We motivate use of this technique,
11 describe a tuning of the underlying phenomenological formula, quantify its performance on fully
12 contained beam-neutrino-induced muon tracks both in simulation and in data, and quantify its
13 performance on exiting muon tracks in simulation. We find agreement between data and simulation
14 for contained tracks, with a small bias in the momentum reconstruction and with resolutions that
15 vary as a function of track length, decreasing from about 10% for the shortest (one meter long)
16 tracks to 5% for longer (several meter) tracks. For simulated exiting muons with at least one meter
17 of track contained, we find a similarly small bias, and a resolution which is less than 15% for muons
18 with momentum below 2 GeV/c though higher at higher momenta.

| | | |
|----|--|----|
| 19 | Contents | |
| 20 | 1 Introduction and motivation | 1 |
| 21 | 2 Multiple Coulomb scattering | 2 |
| 22 | 2.1 Tuning the Highland formula for argon | 4 |
| 23 | 3 MCS implementation using the maximum likelihood method | 6 |
| 24 | 3.1 Track segmentation and scattering angle computation | 7 |
| 25 | 3.2 Maximum likelihood theory | 7 |
| 26 | 3.3 Maximum likelihood implementation | 8 |
| 27 | 4 Range-based energy validation from simulation | 8 |
| 28 | 5 MCS performance on beam neutrino-induced muons in MicroBooNE data | 10 |
| 29 | 5.1 Input sample | 10 |
| 30 | 5.2 Event selection | 10 |
| 31 | 5.3 Validation of the Highland formula | 11 |
| 32 | 5.4 MCS momentum validation | 11 |
| 33 | 5.5 Impact of Highland formula tuning | 12 |
| 34 | 6 MCS performance on exiting muons in MicroBooNE simulation | 15 |
| 35 | 7 Conclusions | 16 |

36 **1 Introduction and motivation**

37 In this paper we summarize the theory of multiple Coulomb scattering (MCS) and describe how the
38 underlying Highland formula is retuned based on Monte Carlo simulation for use in liquid-argon
39 time-projection chambers (LArTPCs). We present a maximum likelihood based algorithm that is
40 used to determine the momentum of particles in a LArTPC. The only way to determine the mo-
41 mentum of a particle that exits the active volume of a LArTPC is through MCS measurements. We
42 demonstrate that this technique works well for a sample of fully contained muons from Booster
43 Neutrino Beam (BNB) ν_μ charged-current (CC) interactions, and determine the resolutions and bi-
44 ases of the measurement. In addition we demonstrate the performance of the method on simulated
45 exiting tracks.

46
47 MicroBooNE (Micro Booster Neutrino Experiment) is an experiment that uses a large LArTPC
48 to investigate the excess of low energy events observed by the MiniBooNE experiment [1] and to
49 study neutrino-argon cross-sections. MicroBooNE is the first detector of the Short-Baseline Neu-
50 trino (SBN) [2] physics program at the Fermi National Accelerator Laboratory (Fermilab), to be

joined by two other LArTPCs: the Short Baseline Near Detector (SBND) and the Imaging Cosmic And Rare Underground Signal (ICARUS) detector [3]. MicroBooNE also performs important research and development in terms of detector technology and event reconstruction techniques for future LArTPC experiments including DUNE (Deep Underground Neutrino Experiment) [4].

55

The MicroBooNE detector [5] consists of a rectangular time-projection chamber (TPC) with dimensions $2.6 \text{ m} \times 2.3 \text{ m} \times 10.4 \text{ m}$ (width \times height \times length) located 470 m away from the Booster Neutrino Beam (BNB) target [6]. LArTPCs allow for precise three-dimensional reconstruction of particle interactions. For later reference, the $z-$ axis of the detector is horizontal, along the direction of the BNB, while the $x-$ direction of the TPC corresponds to the drift coordinate and the $y-$ direction is the vertical direction. The mass of active liquid argon contained within the MicroBooNE TPC volume is 89 tons, out of a total mass of 170 tons.

63

A set of 32 photomultiplier tubes (PMTs) and three planes of wires with 3 mm spacing at angles of 0, and ± 60 degrees with respect to the vertical are located in the TPC for event reconstruction as shown in figure 1. The cathode plane operating voltage is -70 kV. A neutrino in the beam interacts with an argon nucleus and the charged outgoing secondary particles traverse the medium, lose energy and leave an ionization trail. The resulting ionization electrons drift in a 273 V/cm electric field to the wire planes constituting the anode. The passage of these electrons through the first two wire planes induces a signal in them, and their collection on the third plane also generates a signal. These signals are used to create three distinct two-dimensional views (in terms of wire and time) of the event. Combining these wire signals allow for full three-dimensional reconstruction of the event, with PMT signals providing information about the absolute drift ($x-$) coordinate. The boundaries of the fiducial volume used in this analysis are set back from the six faces of the active volume by distances of between 20 and 37 cm, depending on the face, to reduce the impact of electric-field nonuniformities near the edges of the TPC [7]. This volume corresponds to a mass of 55 tons.

78

The Booster Neutrino Beam (BNB) is composed predominantly of muon neutrinos (ν_μ) with a peak neutrino energy of about 0.7 GeV. Some of these neutrinos undergo charge-current ($\nu_\mu\text{CC}$) interactions in the TPC and produce muons and other particles. For muon tracks which are completely contained in the TPC, it is straightforward to calculate their momentum with a measurement of the length of the particle's track, or with calorimetric measurements which come from wire signal size measurements. Around half of the muons from BNB $\nu_\mu\text{CC}$ interactions in MicroBooNE are not fully contained in the TPC, and therefore using a length-based or calorimetry-based method to determine the momenta for these uncontained tracks is not a possibility; the only way to determine their momenta is through MCS.

88

89 2 Multiple Coulomb scattering

90 Multiple Coulomb scattering (MCS) occurs when a charged particle traverses medium and under-
91 goes electromagnetic scattering off of atomic nuclei. This scattering perturbs the original trajectory

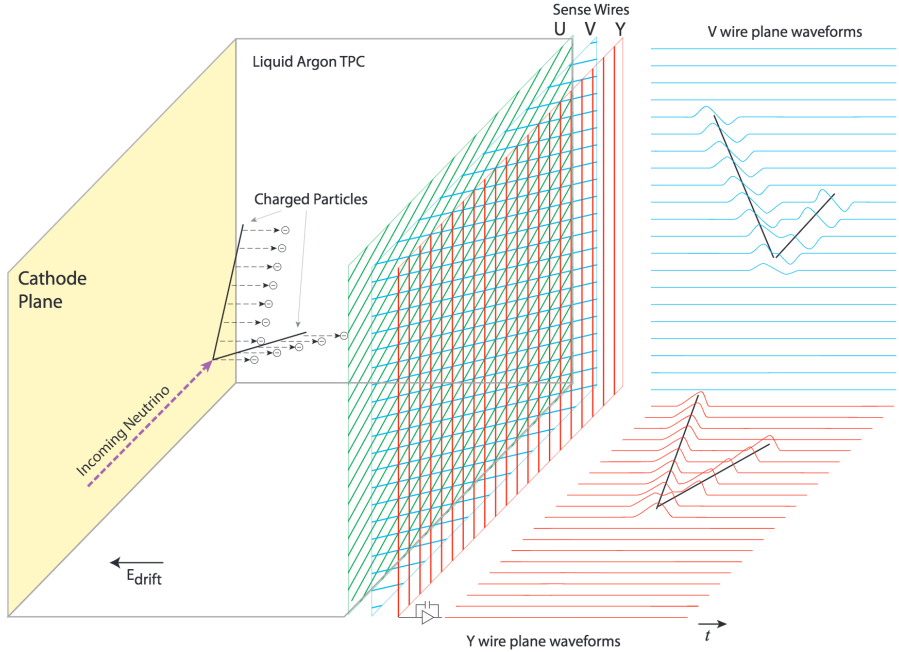


Figure 1. A diagram of the time projection chamber of the MicroBooNE detector [5]. PMTs (not shown) are located behind the wire planes.

of the particle within the material (figure 2). For a given initial momentum p , the angular deflection scatters of a particle in either the x' direction or y' direction (as indicated in the aforementioned figure) form a Gaussian distribution centered at zero with an RMS width, σ_o^{HL} , given by the Highland formula [8][9]

$$\sigma_o^{HL} = \frac{S_2}{p\beta c} z \sqrt{\frac{\ell}{X_0}} \left[1 + \epsilon \times \ln\left(\frac{\ell}{X_0}\right) \right], \quad (2.1)$$

where β is the ratio of the particle's velocity to the speed of light (assuming the particle is a muon), ℓ is the distance traveled inside the material, z is the magnitude of the charge of the particle (unity, for the case of muons), and X_0 is the radiation length of the target material (taken to be a constant 14 cm in liquid argon). S_2 and ϵ are parameters determined to be 13.6 MeV and 0.0038, respectively. In this study, a modified version of the Highland formula is used that includes a detector-inherent angular resolution term, σ_o^{res}

$$\sigma_o = \sqrt{(\sigma_o^{HL})^2 + (\sigma_o^{res})^2}. \quad (2.2)$$

For this analysis, the σ_o^{res} term is given a fixed value of 3 mrad which has been determined to be an acceptable value based on simulation studies muons at higher momenta. At 4.5 GeV/c muon momentum and $\ell \approx X_0$, equation 2.1 predicts an RMS angular scatter of 3 mrad, comparable to the detector resolution. The fully contained muons addressed in this analysis have momenta below 1.5

106 GeV/c, making the impact of this detector resolution minimal for that sample.

107

108 With the Highland formula, the momentum of a track-like particle can be determined using
109 only the 3D reconstructed track information, without any calorimetric or track range information.
110 In neutrino physics experiments, past emulsion detectors like the DONUT [10] and OPERA [11]
111 experiments have used MCS to determine particle momenta. Additionally, the MACRO [12] exper-
112 iment at Gran Sasso Laboratory utilized this technique. The original method for using MCS to de-
113 termine particle momentum in a LArTPC used a Kalman Filter and was described by the ICARUS
114 collaboration [13], and they more recently described another method [14]. The likelihood-based
115 method, discussed in this paper for use in the Microboone detector and described in detail in Sec-
116 tion 3, has improved on the ICARUS method by tuning the underlying phenomenological formula.

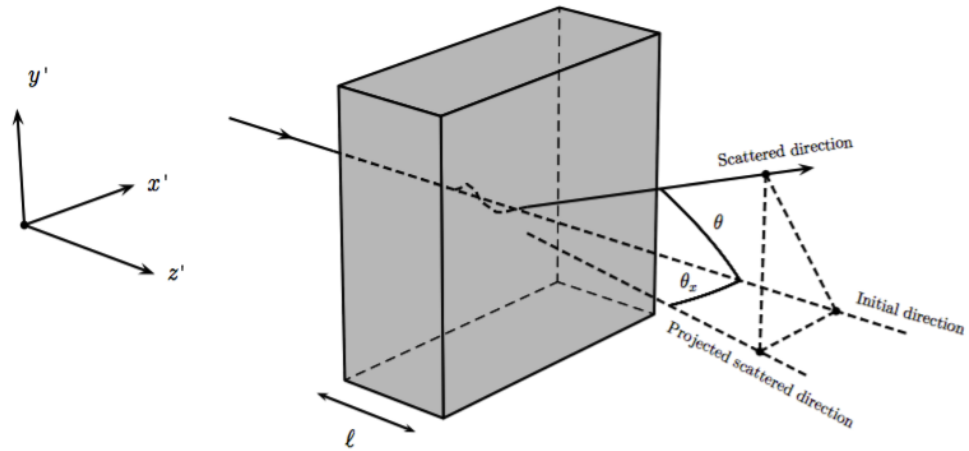


Figure 2. The particle’s trajectory is deflected as it traverses the material.

117 2.1 Tuning the Highland formula for argon

118 The Highland formula as written in equation 2.1 originated from a 1991 publication by G. R. Lynch
119 and O. I. Dahl [9]. The parameters in the equation (S_2 and ϵ) were determined using a global fit
120 over MCS simulated data using a modified GEANT simulation package of 14 different elements
121 and 7 thickness ranges. All of the simulated particles were relativistic, with $\beta = 1$. The materials
122 in which they studied scattering ranged from hydrogen (with $Z=1$) to uranium (with $Z=92$). Given
123 that the parameters in the formula were determined from a single fit to a wide range of Z with a
124 wide range of material thicknesses, there is reason to believe that these parameters should differ
125 for scattering specifically in liquid argon with $l \approx X_0$. There is also reason to believe that these
126 parameters might be momentum-dependent for particles with $\beta < 1$, which is the case for some of
127 the contained muons in this analysis.

128

129 In order to re-tune these parameters to liquid argon, a large sample of muons were simulated
130 with GEANT4 [15] in the MicroBooNE TPC and their true angular scatters were used in a fit,

131 with $l = X_0$. The reason for using $l = X_0$ is that the Highland formula simplifies to remove its
 132 dependence on ϵ

$$\sigma_o^{HL} = \frac{S_2}{p\beta c}. \quad (2.3)$$

133 The S_2 parameter in equation 2.3 was fit for as a function of true muon momentum at each
 134 scatter, in order to explore the β dependence of this parameter. The fitted parameter value as a
 135 function of true momentum is shown in figure 3.

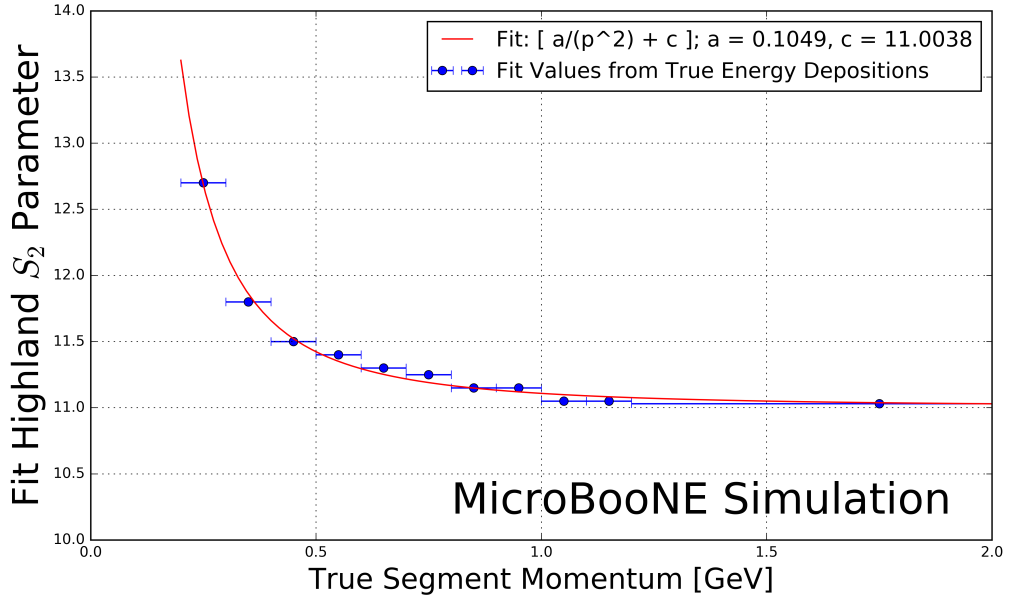


Figure 3. Fitted Highland parameter S_2 as a function of true segment momentum for $\ell = X_0$ simulated muons in the MicroBooNE LArTPC. Blue x- error bars indicate the true momentum bin width with data points drawn at the center of each bin. Shown in red is a fit to these data points with functional form $\frac{a}{p^2} + c$, with best fit values for parameters a and c shown in the legend.

136 It can be seen that the fitted value of S_2 is always less than the nominal 13.6 for momentum
 137 greater than 0.25 GeV/c and asymptotically approaches a constant at higher momentum (where
 138 $\beta = 1$) of about 11.0. The value increases in the momentum region where $\beta < 1$. Shown in red is
 139 a fit to these data points with functional form $\frac{a}{p^2} + c$, with best fit values for floating parameters a
 140 and c being 0.105 and 11.004 respectively. This functional form was chosen because it fit the data
 141 well, and asymptotically approaches a constant value when β approaches 1. This function, used as
 142 a replacement for the S_2 parameter in the Highland formula, will henceforth be referred to as $\kappa(p)$:

$$\kappa(p) = \frac{0.105}{p^2} + 11.004. \quad (2.4)$$

143 To visualize the Highland formula for $\ell = X_0$ both before and after the $\kappa(p)$ replacement,
 144 see figure 4. It is recommended that future LArTPC experiments use this parameterization of the
 145 Highland formula, or at the very least conduct their own studies to tune the Highland formula for

146 scattering in argon. This formulation can also be checked in LAr-based test-beam experiments like
 147 LArIAT [16].
 148

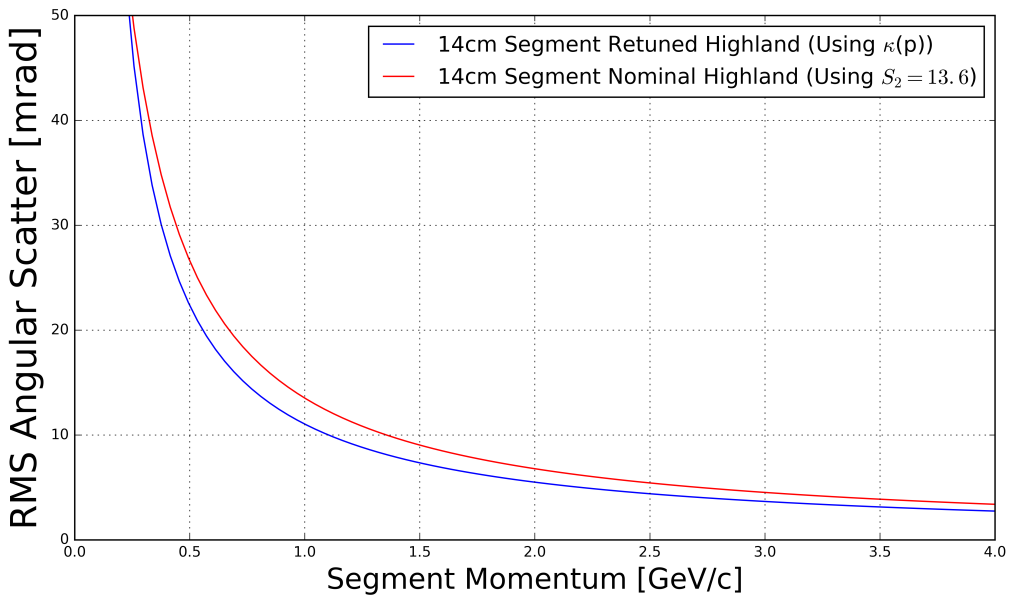


Figure 4. The Highland scattering RMS σ_o for 14 cm segment lengths and 0 detector-inherent angular resolution as a function of true momentum before and after tuning. In red is shown equation 2.3 (the nominal Highland formula using $S_2 = 13.6$) and in blue is the retuned Highland formula (replacing S_2 with $\kappa(p)$).

149 With $\ell = X_0$, the form of the Highland equation used in this analysis is therefore

$$\sigma_o^{RMS} = \sqrt{(\sigma_o)^2 + (\sigma_o^{res})^2} = \sqrt{\left(\frac{\kappa(p)}{p\beta c}\right)^2 + (\sigma_o^{res})^2}. \quad (2.5)$$

150 3 MCS implementation using the maximum likelihood method

151 This section explains exactly how the phenomenon of multiple Coulomb scattering is used to de-
 152 termine the momentum of a muon track reconstructed in a LArTPC. In general, the approach is as
 153 follows:

- 154 1. The three-dimensional track is divided into segments of configurable length.
- 155 2. The scattering angles between consecutive segments are measured.
- 156 3. Those angles combined with the modified, tuned Highland formula (equation 2.5) are used
 157 to build a likelihood that the particle has a specific momentum, taking into account energy
 158 loss in upstream segments of the track.
- 159 4. The momentum corresponding to the maximum of the likelihood is chosen to be the MCS
 160 computed momentum.

161 Each of these steps is discussed in detail in the following subsections.

162

163 3.1 Track segmentation and scattering angle computation

164 Track segmentation refers to the subdivision of three-dimensional reconstructed trajectory points of
165 a reconstructed track into portions of definite length. In this analysis, the tracks are automatically
166 reconstructed by the “pandoraNuPMA” projection matching algorithm [17]. The algorithm con-
167 structs the three-dimensional trajectory points by combining two-dimensional hits reconstructed
168 from signals on the different wire planes along with timing information from the photomultiplier
169 tubes. The segmentation process begins at the start of the track, and iterates through the trajectory
170 points in order, defining segment start and stop points based on the straight-line distance between
171 them. There is no overlap between segments. Given the subset of the three-dimensional trajectory
172 points that corresponds to one segment of the track, a three-dimensional linear fit is applied to the
173 data points, weighting all trajectory points equally in the fit. In this analysis, a segment length of
174 14 cm is used, which is a tunable parameter that has been chosen as described in the derivation of
175 $\kappa(p)$ (equation 2.4).

176

177 With the segments defined, the scattering angles between the linear fits from adjacent segments
178 are computed. A coordinate transformation is performed such that the z' direction is oriented along
179 the direction of the linear fit to the first of the segment pair. The x' and y' coordinates are then
180 chosen such that all of x' , y' , and z' are mutually orthogonal and right-handed, as shown in figure 2.
181 The scattering angles both with respect to the x' direction and the y' direction are then computed to
182 be used by the MCS algorithm. Note that only the scattering angle with respect to the x' direction
183 is drawn in figure 2.

184 3.2 Maximum likelihood theory

185 The normal probability distribution for a scattering angle in either the x' or y' direction, $\Delta\theta$ with
186 an expected Gaussian error σ_o and mean of zero is given by

$$f_X(\Delta\theta) = (2\pi\sigma_o^2)^{-\frac{1}{2}} \exp\left(-\frac{1}{2}\left(\frac{\Delta\theta}{\sigma_o}\right)^2\right). \quad (3.1)$$

187 Here, σ_o is the RMS angular deflection computed by the modified, tuned Highland formula
188 (equation 2.5), which is a function of both the momentum and the length of that segment. Since
189 energy is lost between segments along the track, σ_o increases for each angular measurement along
190 the track so we replace σ_o with $\sigma_{o,j}$, where j is an index representative of the segment.

191

192 To get the likelihood, one takes the product of $f_X(\Delta\theta_j)$ over all n of the $\Delta\theta_j$ segment-to-
193 segment scatters along the track. With some manipulation, this product becomes

$$L(\sigma_{o,1}, \dots, \sigma_{o,n}; \Delta\theta_1, \dots, \Delta\theta_n) = (2\pi)^{-\frac{n}{2}} \times \prod_{j=1}^n (\sigma_{o,j})^{-1} \times \exp\left(-\frac{1}{2} \sum_{j=1}^n \left(\frac{\Delta\theta_j}{\sigma_{o,j}}\right)^2\right). \quad (3.2)$$

194 In practice, rather than maximizing the likelihood it is more computationally convenient to
195 instead minimize the negative log likelihood. Inverting the sign and taking the natural logarithm of

196 the likelihood L gives an expression that is related to a χ^2

$$-l(\mu_o; \sigma_{o,1}, \dots, \sigma_{o,n}; \Delta\theta_1, \dots, \Delta\theta_n) = -\ln(L) = \frac{n}{2} \ln(2\pi) + \sum_{j=1}^n \ln(\sigma_{o,j}) + \frac{1}{2} \sum_{j=1}^n \left(\frac{\Delta\theta_j}{\sigma_{o,j}}\right)^2 \quad (3.3)$$

197 3.3 Maximum likelihood implementation

198 Given a set of angular deflections in the x' and y' directions for each segment as described in
199 Section 3.1 a scan over the postulated initial energy, E_t , in steps of 1 MeV up to 7.5 GeV, and the
200 step with the smallest negative log likelihood (equation 3.3) is chosen as the MCS energy. Note that
201 equation 3.3 includes a $\sigma_{o,j}$ term which changes for consecutive segments because their energy is
202 decreasing. The energy of the j th segment is related to E_t by

$$E_j = E_t - \Delta E_j \quad (3.4)$$

203 where ΔE_j is the energy loss upstream of this segment, computed by integrating the muon
204 stopping power curve given by the Bethe-Bloch equation described by the Particle Data Group
205 (PDG) [19] along the length of track upstream of this segment. Note that equation 3.4 introduces a
206 minimum allowable track energy determined by the length of the track, as E_j must remain positive.
207 This value of segment energy is converted to a momentum, p , with the usual energy-momentum
208 relation assuming the muon mass, and is then used to predict the RMS angular scatter for that
209 segment (σ_o) by way of equation 2.5.

210 4 Range-based energy validation from simulation

211 In order to quantify the performance of the MCS energy estimation method on fully contained
212 muons in data, an additional handle on energy is needed. Range-based energy, E_{range} is used here
213 because the true energy E_{true} will not be known in analyzing detector data. The stopping power of
214 muons in liquid argon is well described by the continuous slowing-down approximation (CSDA)
215 by the particle data group (PDG), and agrees with data at the sub-percent level [18] [20] [21].
216 By using a linear interpolation between points in the cited PDG stopping power table, the length
217 of a track can be used to reconstruct the muon's total energy with good accuracy. A simulated
218 sample of fully contained BNB neutrino-induced muons longer than one meter is used to quantify
219 the bias and resolution for the range-based energy estimation technique. The range is defined as
220 the straight-line distance between the true starting point and true stopping point of a muon, even
221 though the trajectories are not in fact perfectly straight lines. The bias and resolution are computed
222 in bins of true total energy of the muons by fitting a Gaussian to a distribution of the fractional
223 energy difference ($\frac{E_{\text{Range}} - E_{\text{True}}}{E_{\text{True}}}$) in each bin. The mean of each Gaussian yields the bias for that
224 true energy bin, and the width indicates the resolution. Figure 5 shows the bias and resolution for
225 the range-based energy reconstruction method. It can be seen that the bias is negligible and the
226 resolution for this method of energy reconstruction increases slightly with true muon energy but
227 remains on the order of 2-4%. Based on this figure, it is clear that range-based energy (and therefore
228 range-based momentum) is a good estimator of the true energy (momentum) of a reconstructed
229 contained muon track in data, assuming that the track is well reconstructed in terms of length.

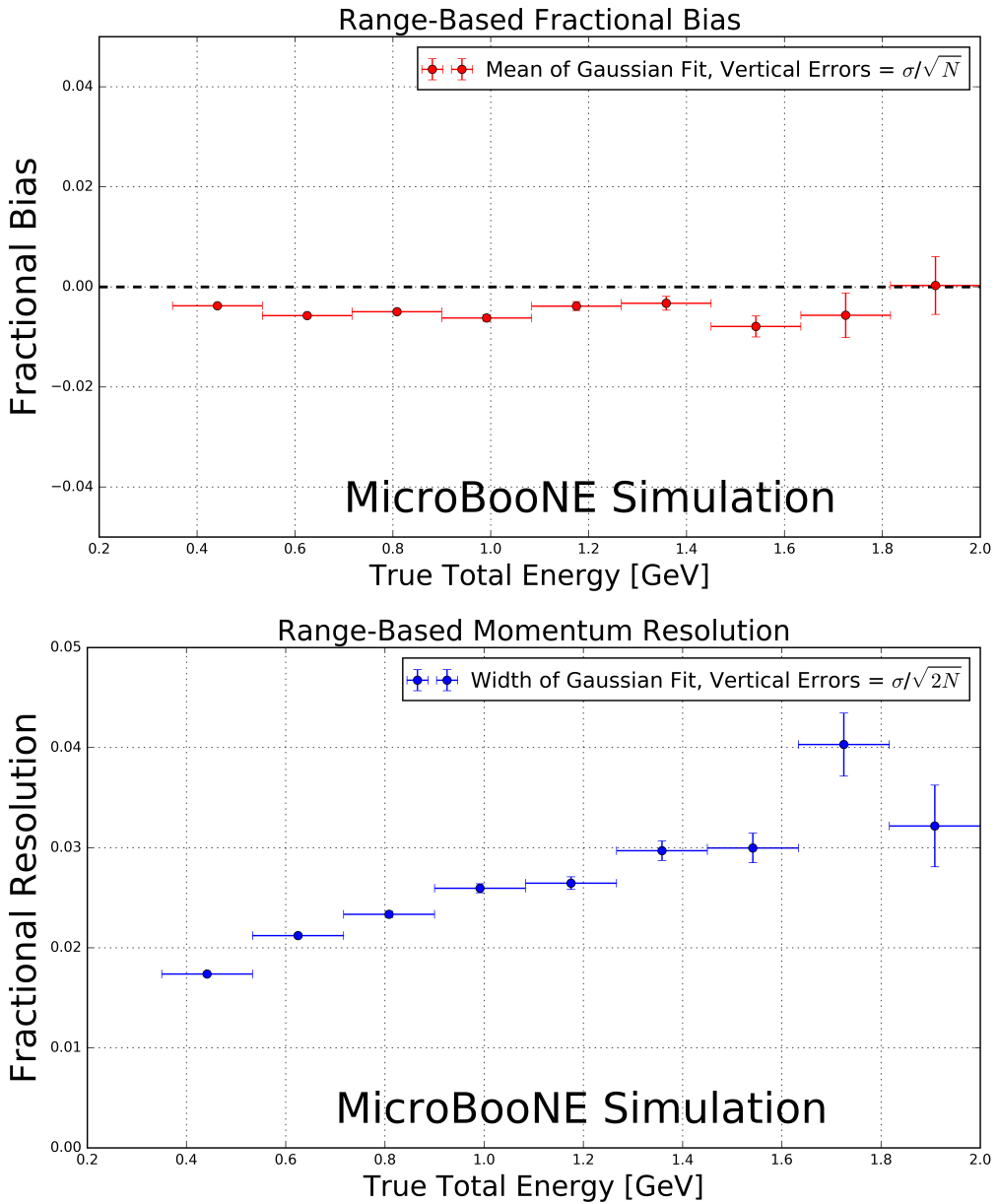


Figure 5. Range-based energy fractional bias (top) and resolution (bottom) from a sample of simulated fully contained BNB neutrino-induced muons using true starting and stopping positions of the track. The bias is less than 1% and the resolution is below $\sim 4\%$.

230 **5 MCS performance on beam neutrino-induced muons in MicroBooNE data**

231 **5.1 Input sample**

232 This part of the analysis is based on triggered neutrino interaction events in MicroBooNE corre-
233 sponding to $\sim 5 \times 10^{19}$ protons on target, which is a small subset (less than 10%) of the nominal
234 amount of beam scheduled to be delivered to the detector. These events are run through a fully
235 automated reconstruction chain that produces reconstructed objects including three-dimensional
236 neutrino interaction points (vertices), three-dimensional tracks (as described in Section 3.1) for
237 each outgoing secondary particle from the interaction, and PMT-reconstructed optical flashes from
238 the interaction scintillation light. The fiducial volume used in this analysis is defined in Section 1.

239 **5.2 Event selection**

240 The following selection cuts are placed on the aforementioned reconstructed objects to select ν_μ
241 charged-current interactions in which a candidate muon track exiting the interaction vertex is fully
242 contained within the fiducial volume:

- 243 1. The event must have at least one bright optical flash, reconstructed from PMT timing signals,
244 in coincidence with the expected BNB-neutrino arrival time.
- 245 2. Two or more reconstructed tracks must originate from the same reconstructed vertex within
246 the fiducial volume.
- 247 3. The position in $z-$ of the optical flash, as determined by the pulse height and timing of
248 signals in the 32 PMTs, must be within 70 cm of some point on the $z-$ projection of the
249 candidate muon track.
- 250 4. For events with exactly two tracks originating from the vertex, additional calorimetric-based
251 cuts are applied to mitigate backgrounds from cosmic muons arriving in time with the pas-
252 sage of the beam which stop and produce a decay electron reconstructed as a track.
- 253 5. The longest track originating from the vertex is assumed to be a muon, and it must be fully
254 contained within the fiducial volume.
- 255 6. The longest track must be at least one meter long, in order to have sufficient sampling points
256 in the MCS likelihood to obtain a reasonable estimate of its momentum.

257 These cuts were chosen to select a sample of tracks with high purity. In this sample of Micro-
258 BooNE data, 598 events (tracks) remain after all event selection cuts. The relatively low statistics
259 in this sample is due to the limited input sample, described in Section 5.1. Each of these events
260 (tracks) was scanned by hand with a 2D interactive event display showing the raw wire signals of
261 the interaction from each wire plane, with the 2D projection of the reconstructed muon track and
262 vertex overlaid. The scanning was done to ensure the track was well reconstructed with start point
263 close to the reconstructed vertex and end point close to the end of the visible wire-signal track in all
264 three planes. During the scanning, we removed obvious mis-identification topologies. An example
265 of such a topology is a stopping cosmic-ray muon decaying into an electron. After we rejected
266 events (tracks) based on hand scanning, 396 tracks remain for analysis.

267 **5.3 Validation of the Highland formula**

268 The Highland formula indicates that histograms of angular deviations of the track, segment by
 269 segment, in both the x' and y' directions divided by the width predicted from the Highland equation
 270 σ_o^{RMS} (equation 2.5) should be Gaussian with a width of unity. In order to calculate the momentum
 271 p in the Highland equation, p for each segment is computed with equation 3.4, where E_t comes
 272 from the converged MCS computed momentum of the track. For each consecutive pair of segments
 273 in this sample of 396 tracks, the angular scatter divided by the Highland expected RMS (including
 274 detector resolution term, σ_o^{res}) is an entry in the area-normalized histogram shown in figure 6.
 275 These 396 tracks have on average 12 segments each, therefore this histogram has approximately
 276 $396 \times 12 \times 2 = 9504$ entries. The additional factor of 2 comes from angular scatters both in the
 277 x' and y' directions. From this figure we can see that the distribution has an RMS of unity, thus
 278 validating the MCS technique used in this analysis.

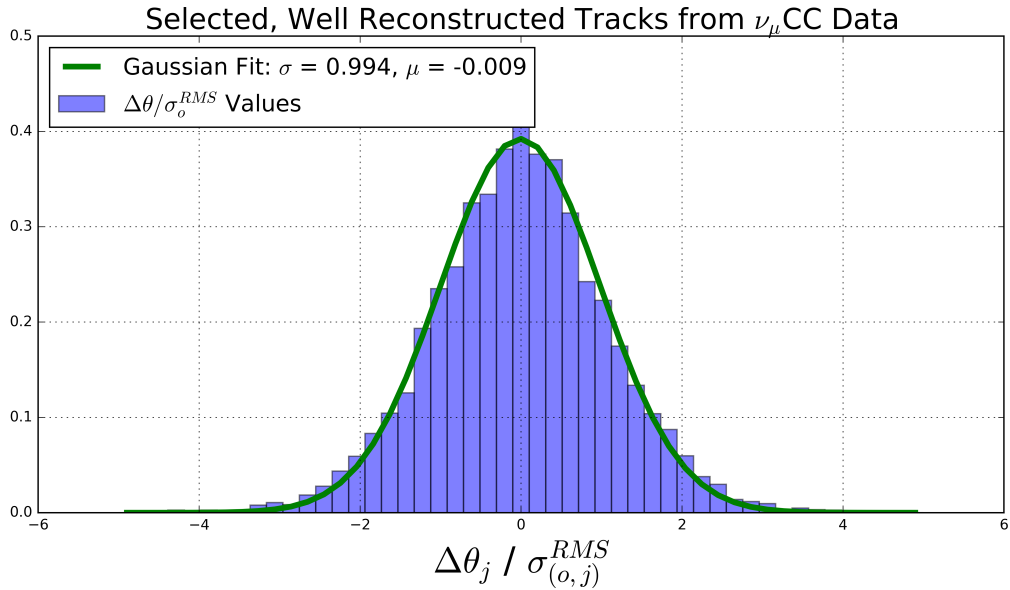


Figure 6. Segment-to-segment measured angular scatters in both the x' and y' directions divided by the Highland formula (equation 2.1) predicted width σ_o^{RMS} for the automatically selected beam neutrino-induced fully contained muon sample in MicroBooNE data after hand scanning to remove poorly reconstructed tracks and obvious mis-identification topologies. That the fitted Gaussian distribution has a width of near unity indicates that the basis of the MCS technique is validated.

279 **5.4 MCS momentum validation**

280 The MCS momentum versus range-based momentum for this sample of 396 tracks can be seen in
 281 figure 7. The fractional bias and resolution as a function of range-based momentum for this sample
 282 is shown in figure 8. In order to compute this bias and resolution, distributions of fractional inverse
 283 momentum difference ($\frac{p_{MCS}^{-1} - p_{Range}^{-1}}{p_{Range}^{-1}}$) in bins of range-based momentum p_{Range} are fit to Gaus-
 284 sians and the mean of the fit determines the bias while the width of the fit determines the resolution
 285 for that bin. Inverse momentum is used here because the binned distributions are more Gaussian

(since the Highland formula measures inverse momentum in terms of track angles that have reasonably Gaussian errors). Note that simply using the mean and RMS of the binned distributions yields similar results. Also shown in this figure are the bias and resolutions for an analogous simulated sample consisting of full BNB simulation with CORSIKA-generated [22] cosmic overlays passed through an identical reconstruction and event selection chain. Rather than hand scanning this sample, true simulation information was used by requiring the longest reconstructed track matched well in terms of true starting and stopping point of the ν_μ CC muon. This removes any mis identifications or interference from the simulated cosmics.

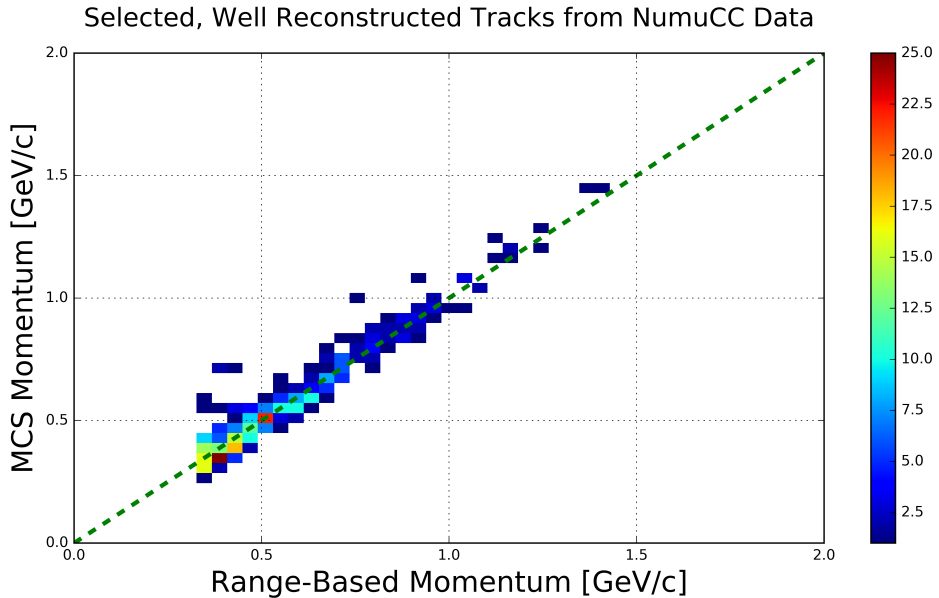


Figure 7. MCS computed momentum versus range momentum for the automatically selected beam neutrino-induced fully contained muon sample in MicroBooNE data after hand scanning to remove poorly reconstructed tracks and obvious mis-identification topologies. The color (z) scale indicates number of tracks.

Figure 8 indicates a bias in the MCS momentum calculation on the order of a few percent, with a resolution that decreases from about 10% for contained reconstructed tracks in data and simulation with range momentum around 0.45 GeV/c (which corresponds to a length of about 1.5 meters) to below 5% for contained reconstructed tracks in data and simulation with range momentum about 1.15 GeV/c (which corresponds to a length of about 4.6 meters). Resolution improving with length of track is intuitive; the longer the track, the more angular scattering measurements can be made to improve the likelihood. In general the bias and resolutions agree between data and simulation within uncertainty.

302

303 5.5 Impact of Highland formula tuning

304 In order to examine the impact of the Highland formula tuning described in Section 2.1, the fractional bias and resolution on the simulated sample of contained muons described in Section 5.4
305 both with the nominal Highland formula (equation 2.2) and with the retuned Highland formula
306

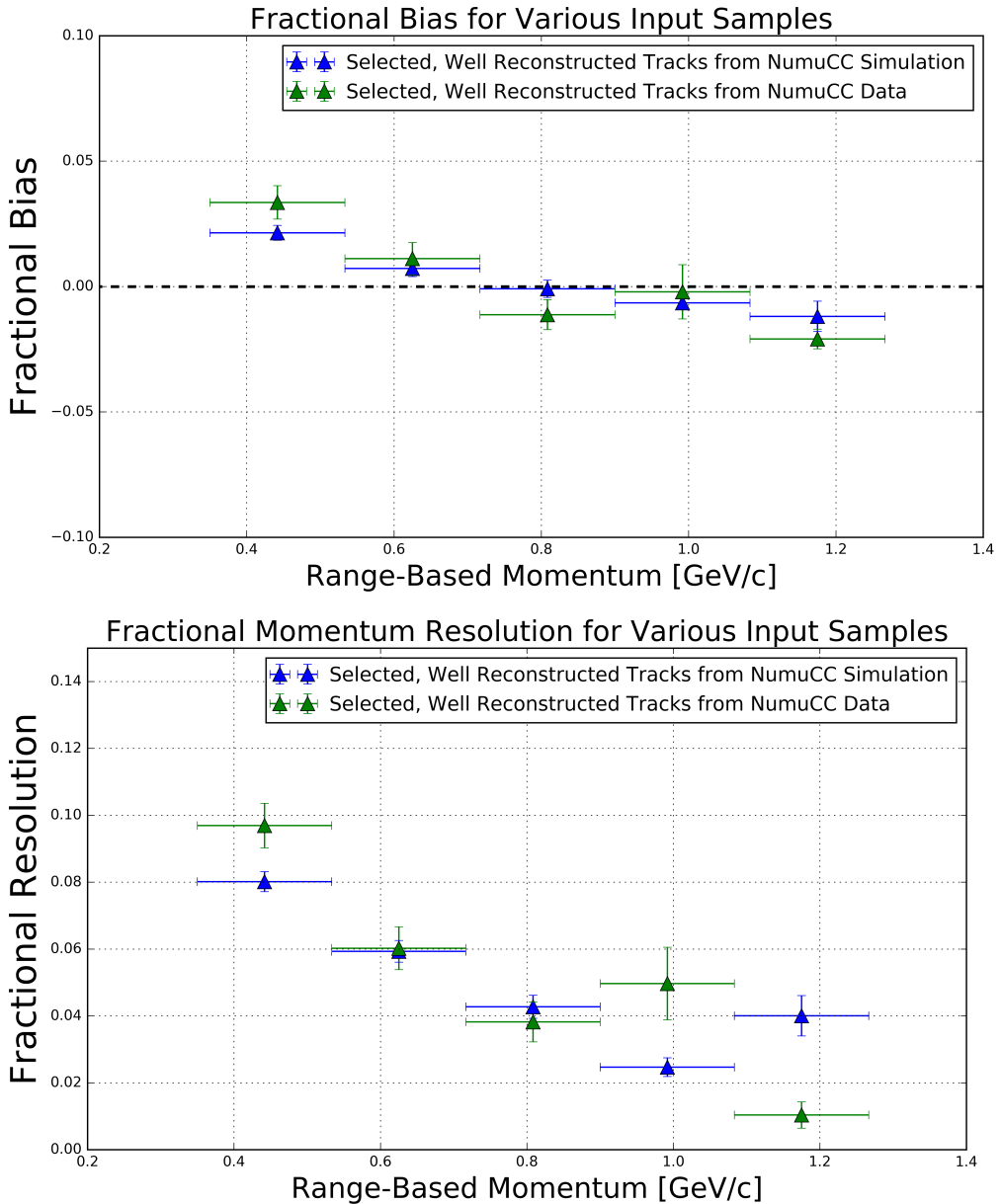


Figure 8. Inverse momentum difference (as defined in the text) fractional bias (top) and resolution (bottom) for automatically selected contained ν_μ CC-induced muons from full simulated BNB events with cosmic overlay where the track matches with the true muon track (blue), and automatically selected (see text) contained ν_μ CC-induced muons from MicroBooNE data (green).

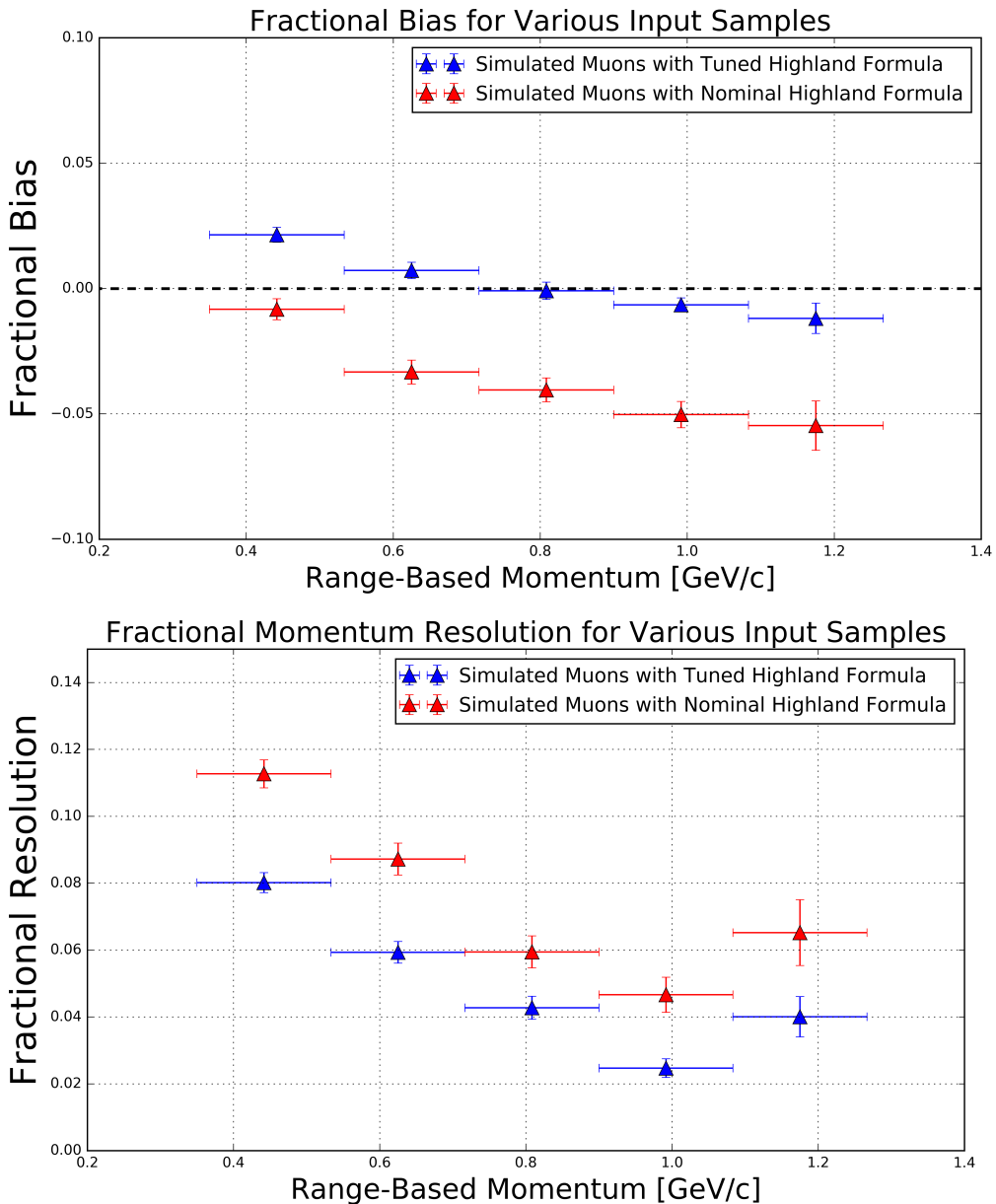


Figure 9. Inverse momentum difference (as defined in the text) fractional bias (top) and resolution (bottom) for automatically selected contained ν_μ CC-induced muons from full simulated BNB events with cosmic overlay where the track matches with the true muon track both using the nominal Highland formula (equation 2.2) (red) and the retuned Highland formula (equation 2.5) (blue).

(equation 2.5) are shown in figure 9. Tuning the Highland formula improves the magnitude of the fractional bias to below 2%, and improves the fractional resolution by 2-3%, with the most improvement in the lowest momentum bins.

310 6 MCS performance on exiting muons in MicroBooNE simulation

311 This section quantifies the MCS algorithm performance on a sample of exiting muon tracks in
 312 simulated BNB ν_μ CC interactions within the MicroBooNE detector. The tracks are automatically
 313 reconstructed by the same “pandoraNuPMA” algorithm described in Section 3.1, and all tracks
 314 have at least one meter contained within the TPC. This simulation does not include space-charge
 315 effects. The MCS momentum versus true momentum at the beginning of the track as given by
 316 simulation for this sample of 28,000 exiting muon tracks can be seen in figure 10.

317

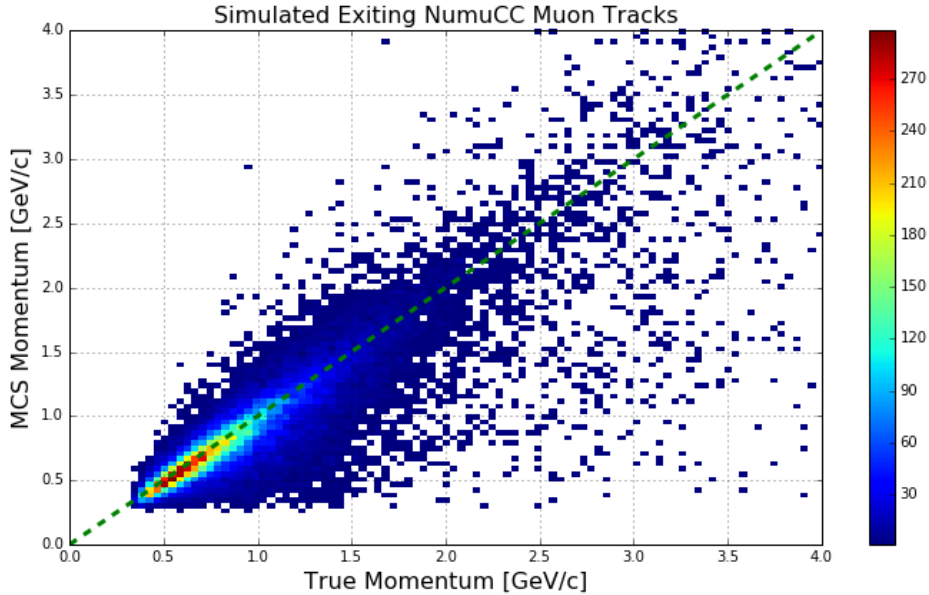


Figure 10. MCS computed momentum versus true momentum for the sample of simulated exiting BNB ν_μ CC muons in MicroBooNE with at least one meter of track contained within the TPC.

318 The distribution of $(\frac{p_{MCS}^{-1} - p_{true}^{-1}}{p_{true}^{-1}})$ is shown for four representative bins of true momentum in
 319 figure 11, along with the Gaussian fit to each. Low-momentum tails in which the MCS momentum
 320 is an underestimation of the true momentum can be seen outside of the central Gaussian fit. These
 321 tails can be attributed to poor track reconstruction effects.

322

323 The fractional bias and resolution as a function of true momentum are shown in figure 12. It
 324 can be seen that the bias is below 4% for all momenta, and the resolution is roughly 14% in the
 325 relevant momentum region for BNB ν_μ CC muons (below 2 GeV/c). The resolution worsens for
 326 muon momenta above this region because the angular scatters begin to be comparable with the
 327 detector resolution term of 3 mrad. Note that the resolution improves for longer lengths of track
 328 contained, with 10% resolution for muons below 2 GeV/c with more than 3.5 meters contained.
 329 The mean length of track contained for muons in this analysis is 212 cm.

330

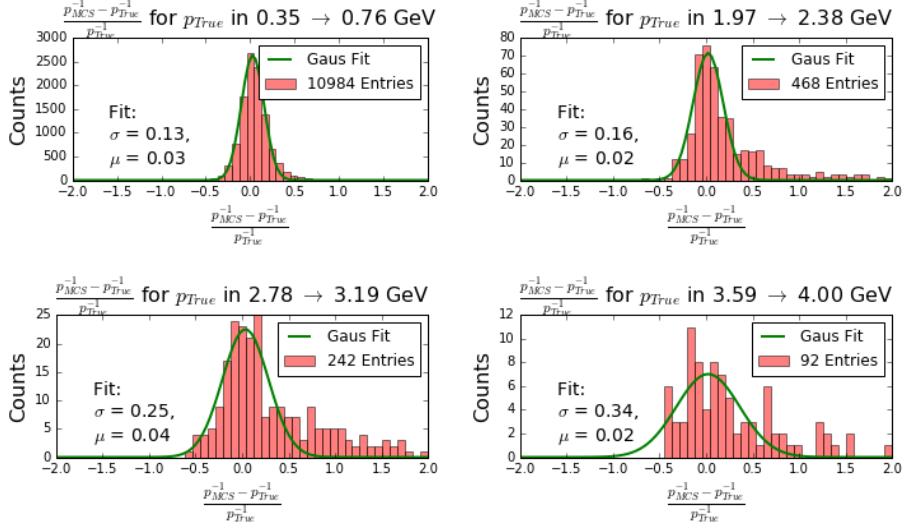


Figure 11. Fractional momentum difference for a few representative bins of true momentum.

331 7 Conclusions

332 We have described a multiple Coulomb scattering maximum likelihood method for estimating the
 333 momentum of a three dimensional reconstructed track in a LArTPC and have provided motivation
 334 for development of such a technique. Using simulation, we have shown that the standard Highland
 335 formula should be re-tuned specifically for scattering in liquid argon. After benchmarking range-
 336 based momentum-determination techniques with MicroBooNE simulation, we have demonstrated
 337 the accuracy and precision of the MCS-based momentum reconstruction in MicroBooNE data
 338 by comparing its performance to the range-based method. For 398 fully-contained BNB ν_μ CC-
 339 induced muons, the MCS method exhibits a fractional bias below 3% and a momentum resolution
 340 below 10%, agreeing with simulation predictions. Using simulation of a separate sample of un-
 341 contained muon tracks in MicroBooNE with at least one meter contained in the active volume,
 342 the MCS-based reconstruction is shown to produce a fractional bias below 4% and a momentum
 343 resolution of better than 15% for muons in the relevant BNB energy region of below 2 GeV.

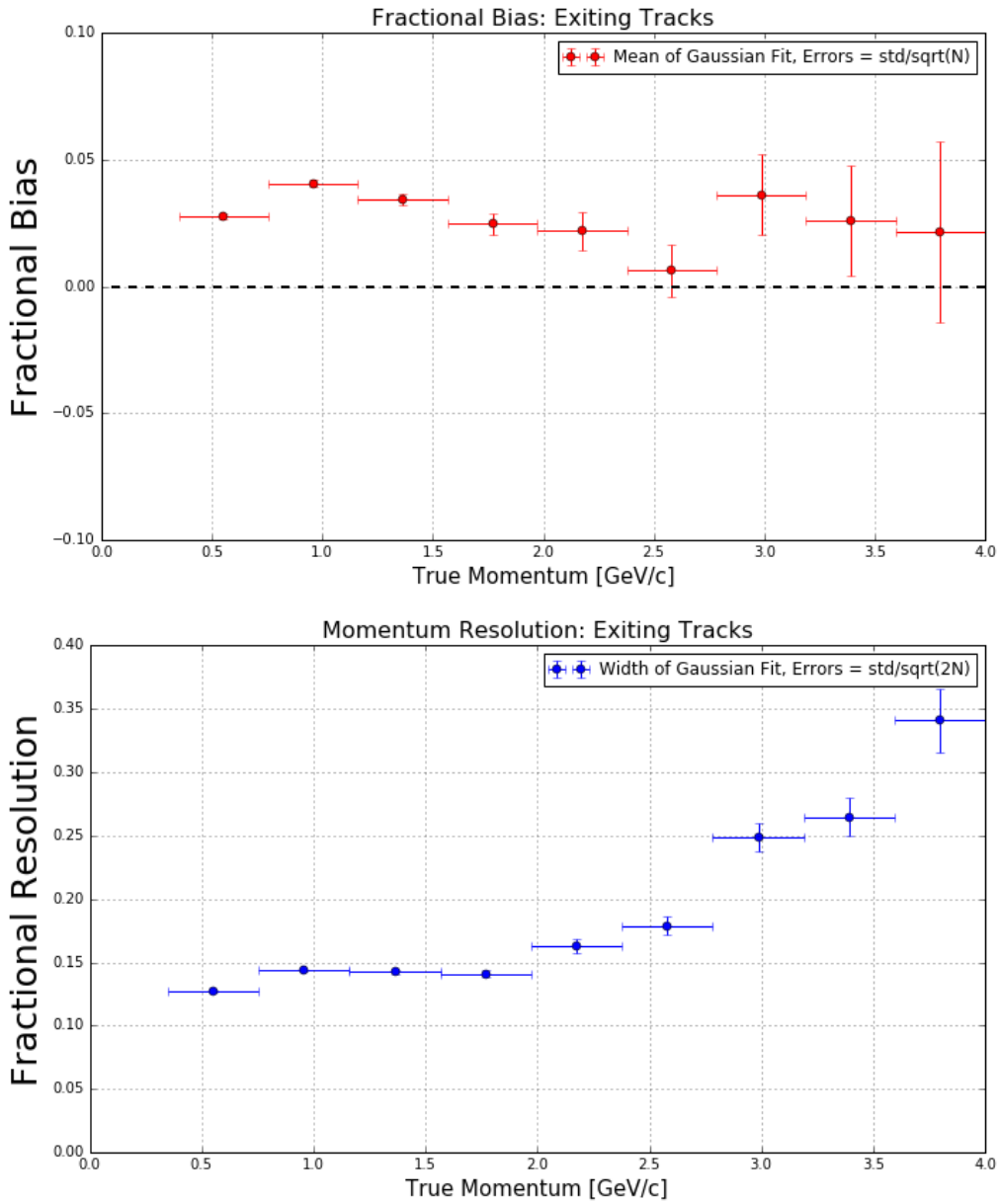


Figure 12. MCS momentum fractional bias (top) and resolution (bottom) as a function of true momentum from a sample of exiting reconstructed muon tracks.

344 **References**

- 345 [1] A. A. Aguilar-Arevalo *et al.* [MiniBooNE Collaboration], Improved Search for $\bar{\nu}_\mu \rightarrow \bar{\nu}_e$ Oscillations
346 in the MiniBooNE Experiment, Phys. Rev. Lett. **110**, 161801 (2013).
347 doi:10.1103/PhysRevLett.110.161801 [arXiv:1207.4809 [hep-ex], arXiv:1303.2588 [hep-ex]].
- 348 [2] C. Adams *et al.* [LArTPC Collaboration], arXiv:1309.7987 [physics.ins-det].
- 349 [3] F. Arneodo *et al.* [ICARUS Collaboration], hep-ex/0103008.
- 350 [4] R. Acciarri *et al.* [DUNE Collaboration], arXiv:1601.05471 [physics.ins-det].
- 351 [5] R. Acciarri *et al.* [MicroBooNE Collaboration], “Design and Construction of the MicroBooNE
352 Detector,” arXiv:1612.05824 [physics.ins-det].
- 353 [6] A. A. Aguilar-Arevalo *et al.* [MiniBooNE Collaboration], Phys. Rev. D **79**, 072002 (2009)
354 doi:10.1103/PhysRevD.79.072002 [arXiv:0806.1449 [hep-ex]].
- 355 [7] R. Acciarri *et al.* [MicroBooNE Collaboration], “Study of Space Charge Effects in MicroBooNE”
356 www-microboone.fnal.gov/publications/publicnotes/MICROBOONE-NOTE-1018-PUB.pdf.
- 357 [8] V. L. Highland, Some Practical Remarks on Multiple Scattering, Nucl. Instrum. Methods **129** (1975)
358 104-120.
- 359 [9] G. R. Lynch and O. I. Dahl, Nucl. Instrum. Methods Section B (Beam Interactions with Materials
360 and Atoms) **B58**, **6** (1991).
- 361 [10] K. Kodama *et al.* [DONUT Collaboration], Phys. Lett. B **504**, 218 (2001)
362 doi:10.1016/S0370-2693(01)00307-0 [hep-ex/0012035].
- 363 [11] N. Agafonova *et al.* [OPERA Collaboration], New J. Phys. **14**, 013026 (2012)
364 doi:10.1088/1367-2630/14/1/013026 [arXiv:1106.6211 [physics.ins-det]].
- 365 [12] G. Giacomelli [MACRO Collaboration], Braz. J. Phys. **33**, 211 (2003)
366 doi:10.1590/S0103-97332003000200008 [hep-ex/0210006].
- 367 [13] A. Ankowski *et al.* [ICARUS Collaboration], “Measurement of through-going particle momentum by
368 means of multiple scattering with the ICARUS T600 TPC,” Eur. Phys. J. C **48**, 667 (2006)
369 doi:10.1140/epjc/s10052-006-0051-3 [hep-ex/0606006].
- 370 [14] M. Antonello *et al.*, “Muon momentum measurement in ICARUS-T600 LAr-TPC via multiple
371 scattering in few-GeV range,” arXiv:1612.07715 [physics.ins-det].
- 372 [15] S. Agostinelli et al. Nucl. Instrum. Methods Phys. Res. **A506250-303** (2003)
- 373 [16] F. Cavanna *et al.* [LArIAT Collaboration], arXiv:1406.5560 [physics.ins-det].
- 374 [17] J. S. Marshall and M. A. Thomson, “The Pandora Software Development Kit for Pattern
375 Recognition,” Eur. Phys. J. C **75**, no. 9, 439 (2015) doi:10.1140/epjc/s10052-015-3659-3
376 [arXiv:1506.05348 [physics.data-an]].
- 377 [18] D. E. Groom, N. V. Mokhov and S. Striganov, “Muon Stopping Power and Range Tables: 10 MeV -
378 100 TeV” Table 5, <http://pdg.lbl.gov/2012/AtomicNuclearProperties/adndt.pdf>
- 379 [19] H. Bichsel, D. E. Groom, S.R. Klein, “Passage of Particles Through Matter” PDG Chapter 27, Figure
380 27.1 <http://pdg.lbl.gov/2005/reviews/passagerpp.pdf>
- 381 [20] Table 289: Muons in Liquid argon (Ar) http://pdg.lbl.gov/2012/AtomicNuclearProperties/MUON_ELOSS_TABLES/muonloss_289.pdf

- 383 [21] “Stopping Powers and Ranges for Protons and Alpha Particles,” ICRU Report No. 49 (1993); Tables
384 and graphs of these data are available at <http://physics.nist.gov/PhysRefData/>
- 385 [22] D. Heck, J. Knapp, J. N. Capdevielle, G. Schatz, T. Throw, *CORSIKA: A Monte Carlo Code to*
386 *Simulate Extensive Air Showers*, Forschungszentrum Karlsruhe Report FZKA 6019 (1998)